

Dalton Transactions

Accepted Manuscript

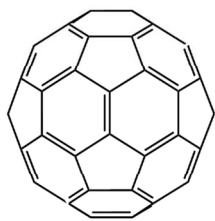


This is an *Accepted Manuscript*, which has been through the Royal Society of Chemistry peer review process and has been accepted for publication.

Accepted Manuscripts are published online shortly after acceptance, before technical editing, formatting and proof reading. Using this free service, authors can make their results available to the community, in citable form, before we publish the edited article. We will replace this *Accepted Manuscript* with the edited and formatted *Advance Article* as soon as it is available.

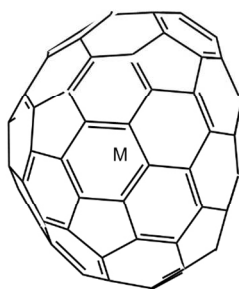
You can find more information about *Accepted Manuscripts* in the [Information for Authors](#).

Please note that technical editing may introduce minor changes to the text and/or graphics, which may alter content. The journal's standard [Terms & Conditions](#) and the [Ethical guidelines](#) still apply. In no event shall the Royal Society of Chemistry be held responsible for any errors or omissions in this *Accepted Manuscript* or any consequences arising from the use of any information it contains.



[60]fullerene

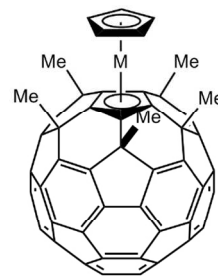
1



M@[82]fullerene

M = La, Er

2 3

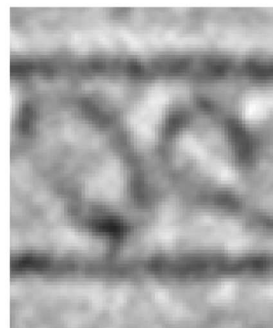
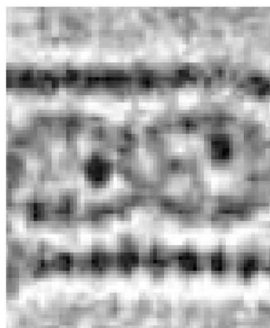
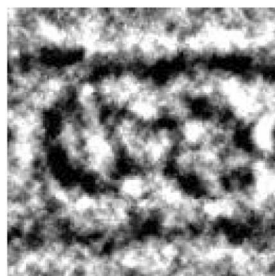
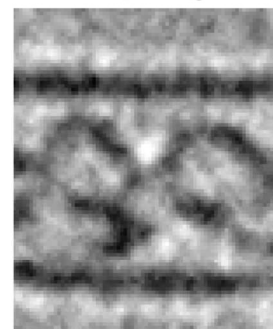
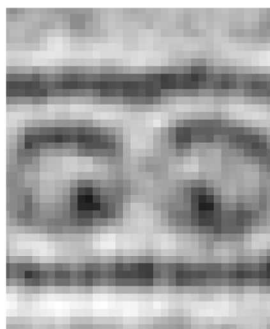
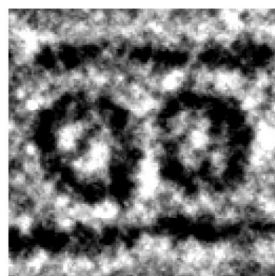


Bucky

metallocene

M = Fe, Ru

4 5



Model structures of Fullerene, endohedral- and exohedral-fullerenes and TEM images before and after the electron beam irradiation.
526x618mm (72 x 72 DPI)

ARTICLE

Multiple Reaction Pathways of Metallofullerenes Investigated by Transmission Electron Microscopy

Cite this: DOI: 10.1039/x0xx00000x

Masanori Koshino ^aReceived 00th January 2012,
Accepted 00th January 2012

DOI: 10.1039/x0xx00000x

www.rsc.org/

Recent advances in molecule-by-molecule transmission electron microscopy (TEM) have provided time-series structural information of individual molecules supported by nano-carbon materials, enabling researchers to trace their motions and reactions. In this paper, the chemical reactions of fullerenes and metallofullerene derivatives, focusing on their deformation process, are reviewed and discussed based on the single-molecule-resolved TEM analysis.

Introduction

Imaging organic molecules by transmission electron microscopy (TEM) has a long history; in other words, it has been a struggle against electron beam damage. Many organic molecules are too sensitive for the molecule-resolved TEM operating conditions¹. A small number of organic crystals are known to preserve rigid crystalline structures under electron beam irradiation, but the majority of interesting organic molecules cannot survive and lose their structural information. Compared to crystals that provide a TEM image as a projection of several molecules, the information of a single organic molecule, such as a carbon atomic chain, is small enough to be veiled under the information of a much thicker substrate.

The emergence of new types of nano-carbon materials, including carbon nanotubes², carbon nanohorns³ and graphene⁴, has prompted us to develop a new analytical technique. A single fullerene molecule encapsulated inside a nanotube has been clearly visualized by TEM, without crystalline formation⁵. The technique has been applied to more fragile organic molecules⁶⁻⁸, not knowing whether they preserve or lose their structural integrity.

A systematic study of single molecules has been performed for a variety of so-called “fragile” organic molecules, either inside or outside nano-carbon materials⁹⁻¹⁴. The state of a single molecule provides a unique environment for suppressing chemical reactions with neighbouring molecules^{13, 15}, which has never been available by any other method. Herein, the chemical reaction of fullerene derivatives will be discussed from a study of [60]fullerene **1**, endohedral [82]fullerene (Er@C₈₂ **2**, La@C₈₂ **3**) and exohedral [60]fullerene (bucky ferrocene **4** and bucky ruthenocene **5**), especially focusing on their deformation process at the presence of metal atoms contained in a molecule (Fig. 1).

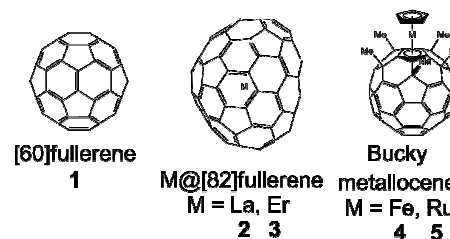


Figure 1. Fullerene, endohedral- and exohedral-fullerenes.

Results and discussion

Dimerisation reaction of [60]fullerene in nanotube.

The dimerisation¹⁶⁻¹⁸ of [60]fullerene molecules occurs inside carbon nanotube ‘peapods’. Within a one-dimensional space, the degrees of freedom are significantly reduced as molecules can undergo translation motion only. The reactions of these molecules are comparable as a function of applied electron dose. In the case of an isolated fullerene molecule observed at 293 K (Fig. 2a) and 793 K (Fig. 2b), no destruction is observed in spite of the molecule being under substantial electron dose and heating. The low reactivity of a single molecule is significantly different from the conventional knowledge of bulk materials where electron-induced reactions deteriorate the specimen structures^{15, 19}.

Fig. 2c-e shows two distinct stages of electron-irradiated C₆₀ transformations in a nanotube: distinguished as ‘phase1’ and ‘phase2’, where bond formations are reversible in phase1, and irreversible fusions are observed in phase2. A time series of C₆₀ dimerisation is shown in Fig. 2c-e. The contrast of C₆₀ molecules is observable after the elimination of the tube lattice, which is enhanced in Fig. 2f-h. The TEM images are simulated, as shown in Fig. 2i-k, based on the models shown in Fig. 2m-o. There are several candidates for the initial orientations of C₆₀

pairs; however, the ability of TEM makes it highly likely to observe molecular structures even during the reaction¹³.

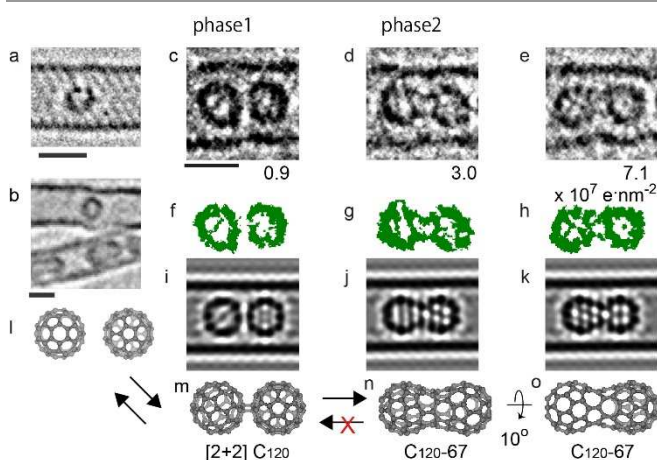


Figure 2. Dimerisation reaction of C_{60} , observed by TEM. When a molecule is isolated, the fullerene maintains its original structure as no dimerisation occurs. Images are recorded at $E=120$ kV and $dose=5.3 \times 10^6$ electrons \cdot nm $^{-2}$ but at different temperatures: (a) $T=293$ K, and (b) $T=793$ K. Contrast inside the fullerene cage indicates the orientation of molecules. (c-e) TEM image. (f-h) Extracted fullerene contrast. (i-k) TEM simulation based on model structures (m-o) are shown as a series of electron doses indicated on the right bottom side of panels (c-e). A bond formation of phase1 is reversible (l, m), whereas phase2 is observed as an irreversible fusion (m, n). A time-series movie revealed that the fused structures (d and e) are explained as 10-degree rotations of the same model structure (n and o). The simulation parameters are: spherical aberration coefficient (C_s)=30 μ m, defocus (Δf)=-10 nm and defocus spread (ds)=5nm. Scale bar indicates 1 nm.

By assuming a [2+2] cyclo-adduct, only a C_{120} dimer with C_s symmetry, in which pentagon and hexagon edges are connected to each other (expressed as $C_{120-56/66}$ (ph)^{20, 21}), provides similar contrast with the TEM image. Although x-ray analysis revealed the crystal structure of a [2+2] cyclo-adduct as a hexagon-hexagon (hh) connected form with D_{2h} symmetry²², it was also pointed out that all four [2+2] isomers could be possible depending on the initial orientation of the molecules rather than their thermodynamic stability²³.

The fused structure in phase2 is shown in Fig. 2d and 2e at electron doses of 3.0×10^7 e $^{-}$ nm $^{-2}$ or greater. Five possible structures of the fused C_{120} molecule^{20, 21} are considered, together with their TEM simulations¹³. After a careful comparison, it is observed that the model structure of C_{120-67} (D_3) provided similar contrast with the present TEM observation. In the model, the hexagon ends of both C_{60} molecules are facing each other and reconnected to the neighbour's hexagons while rotating each molecule by 60 $^\circ$ (see Fig. 2n and 2o). Interestingly, the fused structure in Fig. 2e at an electron dose of 7.1×10^7 e $^{-}$ nm $^{-2}$ can also be explained by the same model, in which the observed contrast is interpreted as a 10 $^\circ$ rotation from the model structure predicted for Fig. 2d. A time-sequential structural characterization provides 3D information on molecules when the molecules spontaneously rotate within a nanotube.

Thus, a high-resolution TEM approach can provide beneficial information about the structure during the reaction. Assuming

that the local structure plays an important role to further advance the reaction, bond formations between C_{60} molecules may have typical facets or apexes towards neighbouring C_{60} molecules.

Reaction of endohedral metallo-[82]fullerene ($M@C_{82}$) in nanotube.

It is well known that a catalyst increases the rate of reactions, but the phenomenon is not fully understood on the basis of a single molecule and a single catalyst until the time of its quantitative analysis¹³. First, it is necessary to mention that the orientation of an unsymmetric $M@C_{82}$ molecule plays an important role in the dimerisation reaction within the narrow space of nanotubes, as seen in Fig. 3a and 3b. Fig. 3a illustrates three tubes (i-iii) containing $Er@C_{82}$ molecules in two different orientations: in tubes i and iii, molecules are packed with their apse (longitudinal) lines almost perpendicular to the nanotube axis (Fig. 3c), while in tube ii, the apse lines are almost in line with the tube axis (Fig. 3d). When the head and tail parts of an oval cage of C_{82} contact each other (tube ii in Fig. 3a), bond formation and fusion proceed. On the other hand, when the body parts of an oval cage are adjacent (tube i and iii in Fig. 3a), then few bonds are formed. The present observation is consistent with the previous study in which the polymerization of unsymmetric C_{70} molecules requires proper alignment within wider nanotubes²⁴. By analogy with the x-ray study of functionalized $La@C_{82}$ dimer²⁵, the bond formation must have occurred on the pentagon site that is not located on the body part (Fig. 3d, blue coloured atoms).

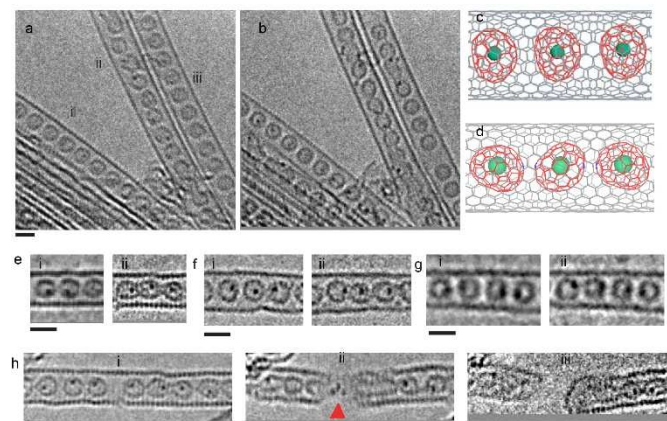


Figure 3. Orientation of molecules in the reactions. (a-b) Reaction of $Er@C_{82}$ selectively progresses in tube ii, observed at $E=80$ kV, $T=293$ K, and $dose=2.1 \times 10^6$ electrons \cdot nm $^{-2}$ (a), 5.7×10^7 electrons \cdot nm $^{-2}$ (b). $Er@C_{82}$ molecules are packed in tubes i and iii as in model (c) and in tube ii as in model (d). C_{82} cages are coloured pink and the closest atoms on the pentagons are coloured blue. (d-f) The existence of metal accelerates fusion with a small electron dose in both the $La@C_{82}$ peapod (e-i: 5.2×10^6 electrons \cdot nm $^{-2}$, e-ii: 5.7×10^7 electrons \cdot nm $^{-2}$) and $Er@C_{82}$ (f-i: 1.1×10^6 electrons \cdot nm $^{-2}$, f-ii: 9.3×10^6 electrons \cdot nm $^{-2}$) observed at $T=293$ K ($C_s \approx 30$ μ m). (g) The specimen stage at 4K (g-i: 2.7×10^5 electrons \cdot nm $^{-2}$, g-ii: 5.4×10^5 electrons \cdot nm $^{-2}$) does not affect the motion of the Er atom in the fullerene cage. The 4K stage reduces the rate of fusion. (h) The La catalysts observed at $E=120$ kV and $T=293$ K effectively cut the nanotube in half with the accumulated electron dose of $\sim 10^7$ electrons \cdot nm $^{-2}$ (h-i: 2.5×10^6 electrons \cdot nm $^{-2}$, h-ii: 9.7×10^6 electrons \cdot nm $^{-2}$, h-iii: 1.1×10^7 electrons \cdot nm $^{-2}$). Scale bars represent 1 nm.

The probability of collisions or interactions between molecules also contributes to the rate of reactions. On the other hand, the filling ratio does not have a significant effect on phase1 and phase2 in Er@C₈₂ molecules in a narrow tube, as the orientation seems to play a more dominant role.

Fig. 3e-h shows TEM images of endohedral metallofullerene peapods and their reactions. The La@C₈₂ peapod, **2**, is observed at 293 K (Fig. 3e), while Er@C₈₂ peapods, **3**, are observed on the specimen stage at 293K (Fig. 3f) and 4 K (Fig. 3g). At experimental conditions of T=293K and E=120 kV, a La@C₈₂ peapod shows bond formations of phase1 at a much smaller electron dose than the metal-free peapod (Table 1). For the fusion process of phase2, both molecule **2** and **3** peapods require smaller electron doses than molecule **1** peapod. Even a single metal atom behaves as a catalyst in the electron-induced transformations. As observed in Fig. 3f, a molecule with a metal atom is highly active under electron beam irradiation at room temperature, but more intact structures of molecules are observed in the sample on the stage at 4K (Fig. 3g). Molecule **3** on the stage at 4 K show less migration of entire molecules than observed in molecule **1** on the stage at the same temperature, which contributes to the lower reactivity. The catalysis-aided reaction of molecule **3** was also examined at E=80 kV¹³. Bond formation and fusion (in phase1 and phase2) of **3** at 80 kV require nearly twice the electron doses than those at 120 kV. In contrast, bond formation and fusion of **1** require 16 times and 9 times higher electron doses, respectively, to react at 80 kV compared to 120 kV. The energy barrier in dimerisation becomes small in the presence of metal atoms, and the initial bond formation and the following fullerene fusion proceed when the orientation is preferable for the reactions.

For molecules **2** and **3**, the required electron doses for reactions were influenced by both the orientation of oval-shape molecules and the presence of a metal atom. The former will contribute positively while the latter may negatively to the electron doses required for chemical reactions.

Table 1 | Electron doses required for fusion of fullerenes at E=120 kV and T=293 K.

Name of molecule	D _{decompose} (e ⁻ ·nm ⁻²) (mean ± s.d.)	
5 Ru(C ₆₀ Me ₅)Cp peapod *	< 1.1 × 10 ⁵	
D _{intra-fusion} (e ⁻ ·nm ⁻²)		
4 Fe(C ₆₀ Me ₅)Cp peapod *	< 2.6 × 10 ⁵	
5 Ru(C ₆₀ Me ₅)Cp peapod *	< 1.6 × 10 ⁶	
D _{phase1} (e ⁻ ·nm ⁻²)		
1 C ₆₀ peapod **	(5.2±2.9) × 10 ⁶	(1.5±0.8) × 10 ⁷
2 La@C ₈₂ peapod **	(7.6±1.2) × 10 ⁵	(1.1±1.4) × 10 ⁷
3 Er@C ₈₂ peapod **	(7.9±6.5) × 10 ⁶	(1.1±0.4) × 10 ⁷

*Nakamura et al.¹⁴, ** Koshino et al.¹³ e⁻·nm⁻² = electrons·nm⁻²

Metal catalysts assist not only the fusion of fullerenes but also the scission of the host nanotube. Under the experimental

conditions E=120 kV and T=293 K, the scission of nanotubes either with or without fullerenes are often observed with substantial electron irradiation doses around 1.0×10⁸ electrons·nm⁻². Fig. 3h shows the breakage of C₈₂ peapods without a metal catalyst at doses of 1.0×10⁸ electrons·nm⁻². The La@C₈₂ peapods, on the other hand, showed an electron-induced scission of the host nanotube at electron doses as small as 1/10 of those required for the metal-free C₈₂ peapod (Fig. 3h). The breakage of the nanotubes depends on many parameters, such as the diameter of the tubes, adsorbates on the tubes, and the chirality of the tubes²⁶. Allowing for large differences in tolerance to electron doses, the presence of La atoms, as indicated by a red arrowhead in Figure 3h-ii, would accelerate the scission of the host tube. Similar phenomena was also reported in Dy@C₈₂ peapods observed by 80 kV- TEM²⁷. The contact of catalysts enhances the formation of new chemical bonds in the carbon network, resulting in an evaporation of carbon atoms from the nanotube so as to cut the tube into two parts.

Reaction of bucky metallocene in nanotube.

Throughout the work of a single-molecule TEM study, it is emphasized that the state of a singly isolated molecule prevents chemical reaction with neighbouring molecules. In the case of two alkyl chains adjacent each other within the same molecule, two separate alkyl chains were visualized without fusion or decomposition over 33.6 sec (6.4×10⁵ electrons·nm⁻², which is 10³ times higher than conventional crystalline destruction of paraffin²⁸). What if the molecule itself has a very active component, such as catalytic metal, inside?

To visualize and characterize a molecule that possesses a catalytic metal atom inside, such as a bucky metallocene, is challenging, because the molecule loses structural integrity with only a small amount of electron beam irradiation¹⁴.

It has been reported that a larger graphitic structure such as C₇₀ can be grown unimolecularly from the two exohedral [60]fullerene derivatives, **4**²⁹ and **5**³⁰ (C₇₀H₂₀Fe = bucky ferrocene, and C₇₀H₂₀Ru = bucky ruthenocene), which requires a much smaller dose to form tubular structures than does C₆₀ or the endohedral f-block transition metal fullerene complexes, M@C₈₂¹³. A single catalytic atom or the structure of bucky metallocenes are capable of incorporating feedstock molecules into a pre-existing graphene network or fusing the fullerene to an existing graphene network, going through various pathways. This finding suggests that a single metal atom, while invisible by usual analyses, might be acting as a catalyst at the site of graphene growth, and suggests also that meticulous control of catalytic graphene growth by a custom-designed single metal catalyst may be possible.

Bucky metallocene compounds **4** (Fe) and **5** (Ru) are the model systems that contain one metal atom and two model feedstocks, one cyclopentadienide (Cp) and five methyl groups. It is likely that the iron or ruthenium atom contributed to the C–C bond cleavage, and the formation produced the volatiles.

Fig. 4a shows a TEM image of 23 molecules of bucky metalloocene compound **4** (Fe) as a peapod on the stage at 4 K, the molecules numbered from left=1 to right=23.

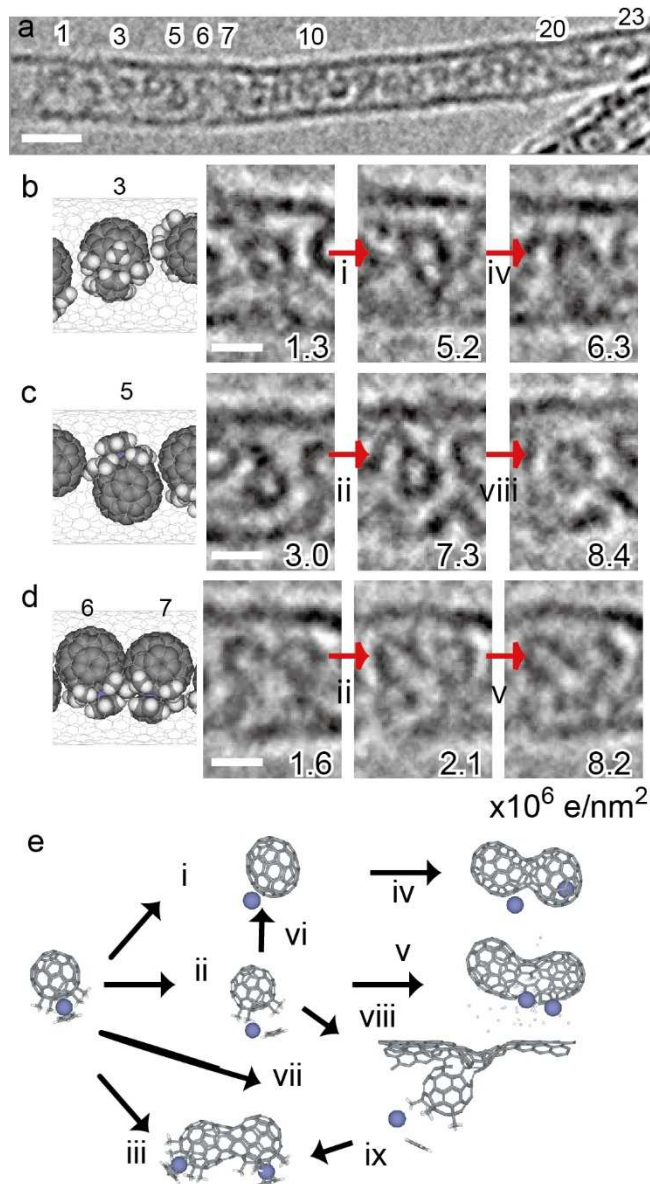


Figure 4. Cryo TEM images of molecule **4**=Fe(C₆₀Me₅)Cp inside a nanotube and reaction analysis of individual molecules. (a) Twenty-three molecules are aligned one-dimensionally along the tube axis recorded at 7.5×10^5 electrons·nm⁻². Each molecule is numbered from left (=1) to right (=23). Scale bar represents 5 nm. (b-d) The courses of the chemical reactions: (b) intramolecular fusion, (c) decomposition followed by reaction with the tube wall, and (d) intermolecular fusion through decomposition, are shown respectively with their model structure on the leftmost figure. Five continuous images are averaged and shown with their recorded electron doses at the bottom. Scale bars represent 1 nm. (e) Some possible chemical reactions of Fe(C₆₀Me₅)Cp are illustrated.

The compartmental tight packing of many molecules of **4** in a 2-nm carbon nanotube was ideal for the study of the reactivity of an organic molecule with a single iron atom, because the iron atom (diameter 0.3 nm) should stay in the compartment even though the C-Fe bond may be cleaved during the reaction. Indeed, during the TEM observation period of 10-20 s, there

was no sign of iron atom clusters that might result from metal atom migration within a tube.

Table 2 | Average electron doses required for reaction events occurred on **4**=Fe(C₆₀Me₅)Cp peapod. Observed at E = 120 kV and T = 4 K (n = 23).

	Dose* (electrons·nm ⁻²) (mean ± s.d.)	Ratio
Decomposition	$(3.0 \pm 2.9) \times 10^6$	17.4%
Intra-molecular fusion	$(4.0 \pm 2.2) \times 10^6$	17.4%
Inter-molecular fusion	$(5.3 \pm 1.5) \times 10^6$	17.4%
Fusion with tube defect	$(5.6 \pm 3.9) \times 10^6$	8.7%
Remain intact	$> 9.3 \times 10^6$	30.4%
Unidentified	n/a	13.0%

* Dose rate = 1.5×10^5 e·nm⁻².

Table 3 | Ratio of observed reaction events occurring on **4**=Fe(C₆₀Me₅)Cp peapod. Observed at E = 120 kV and T = 4 K (n = 23).

Event	Number	Ratio
Remain intact	7	30.4%
Intermolecular fusion (iii)	4	17.4%
Decomposition (ii)	3	13.0%
Intra - inter (i-iv)	3	13.0%
Decomp - intra - inter (ii-vi-iv)	1	4.3%
Decomp - inter (ii-v)	1	4.3%
Intramolecular fusion (i)	1	4.3%
Decomp - tube (ii-viii)	1	4.3%
Tube - inter (vii - ix)	1	4.3%
Unidentified	1	4.3%
Total	23	100.0%

dose rate = 1.5×10^5 electrons·nm⁻², inter = intermolecular fusion, decomp = decomposition, intra = intramolecular fusion, tube = connection with a tube defect.

Of 23 observed molecules, 7 appeared to remain unchanged until receiving an electron dose of 9.3×10^6 electrons·nm⁻² (Table 2). Although 1 out of 23 molecules could not be fully interpreted, a combination of nine different reaction pathways was identified for the remaining 15 molecules, occurring competitively at a similar rate (Fig. 4e and Table 3). For instance, molecule 3, modelled in the left illustration of Figure 4b, rotated slightly and transformed into an oval cage at 5.2×10^6 electrons·nm⁻² (reaction pathway i), resembling C₇₀, and then connected to the neighbouring molecule (iv). Molecule 5 (Fig. 4c) decomposed at 7.3×10^6 electrons·nm⁻² (ii) and then connected to a defect in the tube wall, as seen in the next image at 8.4×10^6 electrons·nm⁻² (viii). Such a decomposition with small electron doses is expected generally for ferrocene derivatives³⁴. The reaction with the defective tube wall was previously reported in the case of C₆₀ observed at 4K.¹³ Figure 4d, with molecules 6 and 7, showed signs of decomposition at 1.6×10^6 electrons·nm⁻² (ii) and fused together

in the next image (v). It is interesting to note that the final product through the chemical reaction is an elongated tubular structure.

Next, the chemical reaction of a 4 peapod at 293K stage is examined by TEM, as shown in Fig. 5a-d. There are four molecules of 4 aligned in a nanotube as shown.

The orientation of two molecules in the middle provides similar contrast as expected in the molecular orientation within a crystal. The crystal structure of 4 along the [110] direction is shown with the multiple unit cells of ($a \times b \times c = 3 \times 3 \times 1$) in Fig. 5e²⁹. When the molecules 4 in the [110] direction are placed inside a (20, 8) nanotube that has a diameter of 1.96 nm, as shown in Fig. 5f, the nanotube provides adequate space for molecule 4, as displayed by van der Waals radii along the tube axis in Fig. 5g, as displayed by van der Waals radii along the tube axis in Fig. 5g. The observed orientations and intermolecular distance of the molecules 4 in Fig. 5a are almost same as the molecular arrangement along the [110] direction within a crystal modelled and simulated in Fig. 5h and 5i. Although a similar orientation was found as a pair of molecules, no long-range order of arrangement was found in a nanotube, even in the specimen on the stage at 4 K.

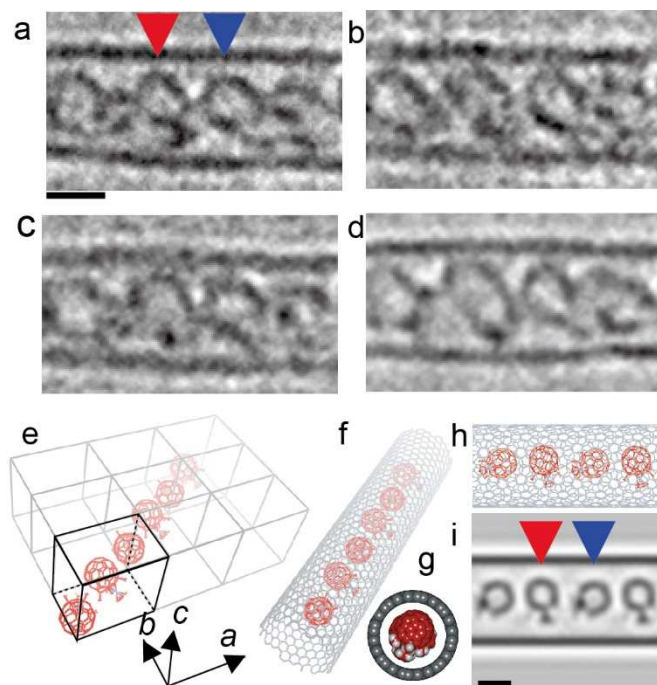


Figure 5. Chemical reaction process of 4 in a nanotube observed by TEM. (a-d) TEM images are taken at 3.7×10^4 electrons \cdot nm $^{-2}$ (a), 2.2×10^5 electrons \cdot nm $^{-2}$ (b), 3.0×10^5 electrons \cdot nm $^{-2}$ (c), 1.6×10^6 electrons \cdot nm $^{-2}$ (d) of accumulated electron doses. A scale bar represents 1nm. (e) The crystal structure of 4 along the [110] direction is shown with the multiple unit cells of ($a \times b \times c = 3 \times 3 \times 1$). (f) The molecules 4 aligned to [110] are placed inside a (20, 8) nanotube (diameter = 1.96 nm). (g) A 4 peapod is displayed by van der Waals radii along the tube axis. (h, i) The peapod structure and its simulated TEM image are shown.

The reaction of the molecule 4 marked with a red arrow in Fig. 5a shows intra-molecular fusion. The clearly visible molecule 4 started to fuse itself after an electron dose of 2.2×10^5 electrons \cdot nm $^{-2}$ (Fig. 5b and Table 1), which apparently requires a much smaller electron dose compared to phase 1 of molecule

1 and the molecule on the 4 K stage (c.f. Table 1 and 2). An ellipsoidal image, reminiscent of higher numbered fullerene, appeared in the image Fig. 5c. In Fig. 5d, the tubulene structure grows with further reaction to absorb other feed stocks, probably from a neighbouring molecule with an accumulated electron dose.

Another molecule 5 with a ruthenium atom, also belonging to a group of eight, was observed by TEM at 293K as a form of nanotube, showing two typical reactions: decomposition and unimolecular (intramolecular) fusion (Fig. 6). When the molecule was isolated in a nanotube, it showed a decomposition reaction, as shown in Fig. 6a. A plate-like moiety, probably Cp, of 5 was apparently removed from the molecule. In another case, an elongated tubular structure formed after a unimolecular fusion reaction, as shown in Fig. 6b. The initial product on the left of Fig. 6b is slightly larger than C₆₀ and more similar to C₇₀ skewed from D_{5h} symmetry, as was observed in molecule 4 in Figs. 4 and 5. The TEM images of molecule 5 in a nanotube are simulated, as Fig. 6c and 6d, based on the model structures of the intact form (left), to illustrate decomposition and unimolecular fusion (Fig. 6e and 6f). High reactivity of bucky metallocenes is remarkable compared to the previous study of alkyl carboranes¹⁵, amide¹⁰ and peptides¹², as well as other fullerene derivatives in a nanotube studied here on a room temperature stage, where molecules retain their skeleton structures up to an electron dose of 10^6 - 10^7 electrons \cdot nm $^{-2}$ under the same experimental conditions. The result of smaller electron dose required for molecule 4 and 5 can be explained by the intrinsic sandwich structure of bucky metallocene molecules and/or the presence of 3d transition metal atom of group 8. The presence of catalytic metal atoms may create new chemical pathways, unpredictable for the conventional organic syntheses^{31, 32}.

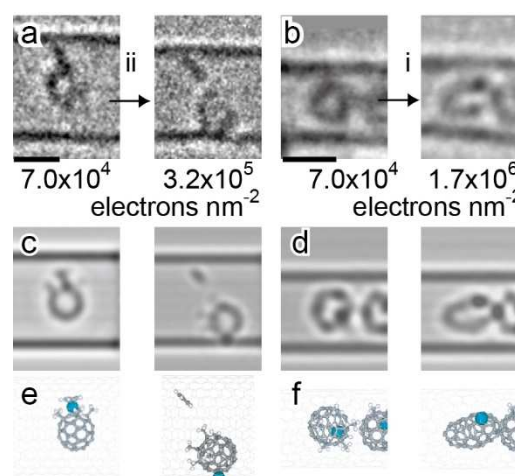


Figure 6. Chemical reaction process of molecule 5=Ru(C₆₀Me₅)Cp peapod observed by TEM. (a, b) TEM images at the beginning of recording (7.0×10^4 electrons \cdot nm $^{-2}$) and after electron irradiation of 3.2×10^5 electrons \cdot nm $^{-2}$ and 1.7×10^6 electrons \cdot nm $^{-2}$ show structural transformation of decomposition (a) and bimolecular (intramolecular) fusion (b), respectively. Scale bars represent 1nm. (c, d) The TEM image simulations based on the model structures indicate decomposition (e) and unimolecular (intramolecular) fusion (f).

Conclusions

Confinement of molecules in a narrow nanotube provides a unique environment by limiting the molecular arrangement in one dimension, enabling us to investigate multiple reaction pathways. Among molecules **1-5**, it is not straight forward to compare the reactivity of molecules due to the differences in numbers of carbon atoms (C_{60} , C_{70} , and C_{82}), molecular shape (sphere, endohedral oval or exohedral) and contained metal atoms (4f block and 3d-group 8 transition metals). Nonetheless, it is beneficial to compare the reactivity of these molecules quantitatively by measuring electron doses, visualizing individual molecules and tracing contained metal behaviours.

In molecule **1** (C_{60}), the experimental TEM conditions operated above threshold energy of fullerene ($20\text{kV} < E$)³³ imparts enough energy for C-C bond to reorganize the structures as phase 1 and phase 2. The energy barrier of phase 1 and phase 2 appears to be sensitive to the incident electron beam as a larger electron dose was necessary to observe bond reorganization at 80 kV. For molecules **2** and **3**, mismatch of orientation suppress the reaction while the presence of metal accelerates the reaction. For molecules **4** and **5**, multiple reaction pathways have been observed as unimolecular (intramolecular) fusion and decomposition with electron dose of $\sim 10^5$ electrons $\cdot\text{nm}^{-2}$: much smaller than the dose required for phase 1 of molecule **1**. The result can be explained by the structure of molecules **4** and **5** and/or the presence of 3d transition metals. Different from molecule **2** and **3**, both factors would contribute negatively to the electron dose: smaller dose is enough for chemical reaction. The structure of molecule and the presence of d-transition metal play an important role to induce intramolecular fusion, decomposition of molecules, and intermolecular fusion with adjacent molecules. It is likely that the oxidation state of metal atom in **4** and **5** reduced from 2 to 0 during the transformation process, similar to the classical oxidative addition and reduction elimination pathway. Such changes in electronic configurations may result in deformation of structure into energetically more stable structures: more detail interpretation requires the aide of theoretical approaches.

Multiple reaction pathways can be thus characterized with molecule-by-molecule TEM under well-controlled experimental conditions. Further efforts for finely tuning the experimental conditions such as adequate beam energy for imaging and controlled temperature and molecular arrangements will provide more beneficial and exciting information for the analysis of reaction pathways based a single molecule study. To understand the reactivity of molecules in detail, theoretical study will elucidate the role of metal atom, which is essential to understand the reactivity of these organometallic compounds.

Acknowledgements

I would like to show my greatest appreciation to Dr. K. Suenaga at AIST, and Prof. E. Nakamura at the Univ. Tokyo, whose comments and suggestions were of inestimable value for my research. I also owe a very important debt to Profs. Y.

Matsuo at the Univ. Tokyo, Profs. T. Okazaki, H. Kataura, and T. Saito at AIST, who contributed high quality specimen provisions for my work. I acknowledge Ms. Y. Niimi at AIST for her excellent TEM work, and Drs. I. Ishikawa and Y. Kondo at JEOL Co. for the development of cryo-TEM. This study was partly supported by MEXT (KAKENHI # 23681026 and #22000008), and Kenkyu-Kasoku-JST.

Notes and references

^a Nanotube Research Centre, National Institute of Advanced Industrial Science and Technology, AIST Central 5, 1-1-1 Higashi, Tsukuba 305-8565, JAPAN.

1. R. F. Egerton, P. Li and M. Malac, *Micron*, 2004, 35, 399-409.
2. S. Iijima, *Nature*, 1991, 354, 56-58.
3. S. Iijima, M. Yudasaka, R. Yamada, S. Bandow, K. Suenaga, F. Kokai and K. Takahashi, *Chem. Phys. Lett.*, 1999, 309, 165-170.
4. K. S. Novoselov, A. K. Geim, S. V. Morozov, D. Jiang, Y. Zhang, S. V. Dubonos, I. V. Grigorieva and A. A. Firsov, *Science*, 2004, 306, 666-669.
5. B. W. Smith, M. Monthieux and D. E. Luzzi, *Nature*, 1998, 396, 323 - 324.
6. T. Takenobu, T. Takano, M. Shiraishi, Y. Murakami, M. Ata, H. Kataura, Y. Achiba and Y. Iwasa, *Nat. Mater.*, 2003, 2, 683-688.
7. D. A. Britz, A. N. Khlobystov, J. Wang, A. S. O'Neil, M. Poliakoff, A. Ardavan and G. A. D. Briggs, *Chem. Commun.*, 2004, 176-177.
8. Z. Liu, M. Koshino, K. Suenaga, A. Mrzel, H. Kataura and S. Iijima, *Phys. Rev. Lett.*, 2006, 96, 088304.
9. M. Koshino, T. Tanaka, N. Solin, K. Suenaga, H. Isobe and E. Nakamura, *Science*, 2007, 1138690.
10. N. Solin, M. Koshino, T. Tanaka, S. Takenaga, H. Kataura, H. Isobe and E. Nakamura, *Chem. Lett.*, 2007, 36, 1208-1209.
11. M. Koshino, N. Solin, T. Tanaka, H. Isobe and E. Nakamura, *Nat. Nanotechnol.*, 2008, 3, 595-597.
12. E. Nakamura, M. Koshino, T. Tanaka, Y. Niimi, K. Harano, Y. Nakamura and H. Isobe, *J. Amer. Chem. Soc.*, 2008, 130, 7808-7809.
13. M. Koshino, Y. Niimi, E. Nakamura, H. Kataura, T. Okazaki, K. Suenaga and S. Iijima, *Nat. Chem.*, 2010, 2, 117-124.
14. E. Nakamura, M. Koshino, T. Saito, Y. Niimi, K. Suenaga and Y. Matsuo, *J. Am. Chem. Soc.*, 2011, 133, 14151-14153.
15. M. Koshino, T. Tanaka, N. Solin, K. Suenaga, H. Isobe and E. Nakamura, *Science*, 2007, 316, 853.
16. A. M. Rao, P. Zhou, K. A. Wang, G. T. Hager, J. M. Holden, Y. Wang, W. T. Lee, X. X. Bi, P. C. Eklund, D. S. Cornett, M. A. Duncan and I. J. Amster, *Science*, 1993, 259, 955-957.
17. B. W. Smith, M. Monthieux and D. E. Luzzi, *Chem. Phys. Lett.*, 1999, 315, 31-36.
18. E. Hernandez, V. Meunier, B. W. Smith, R. Rurali, H. Terrones, M. BuongiornoNardelli, M. Terrones, D. E. Luzzi and J.-C. Charlier, *Nano Lett.*, 2003, 3, 1037-1042.
19. T. Fuller and F. Banhart, *Chem. Phys. Lett.*, 1996, 254, 372-378.
20. D. L. Strout, R. L. Murry, C. Xu, W. C. Eckhoff, G. K. Odom and G. E. Scuseria, *Chem. Phys. Lett.*, 1993, 214, 576-582.
21. M. V. Diudea and C. L. Nagy, *Periodic Nanostructures*, Springer, Dordrecht, Netherlands, 2007.
22. G.-W. Wang, K. Komatsu, Y. Murata and M. Shiro, *Nature*, 1997, 387, 583-586.

23. P. W. Fowler, D. Mitchell, R. Taylor and G. Seifert, *J. Chem. Soc., Perkin Trans. 2*, 1997, 1901-1905.
24. M. Chorro, J. Cambedouzou, A. Iwasiewicz-Wabnig, L. Noé, S. Rols, M. Monthieux, B. Sundqvist and P. Launois, *EPL*, 2007, 79, 56003.
25. L. Feng, T. Tsuchiya, T. Wakahara, T. Nakahodo, Q. Piao, Y. Maeda, T. Akasaka, T. Kato, K. Yoza, E. Horn, N. Mizorogi and S. Nagase, *J. Amer. Chem. Soc.*, 2006, 128, 5990-5991.
26. J. H. Warner, F. Schäffel, G. Zhong, M. H. Rummeli, B. Büchner, J. Robertson and G. A. D. Briggs, *ACS Nano*, 2009, 3, 1557.
27. A. Chuvilin, A. N. Khlobystov, D. Obergfell, M. Haluska, S. Yang, S. Roth and U. Kaiser, *Angew. Chem. Int. Ed.*, 2010, 49, 193-196.
28. R. M. Glaeser, in *Physical Aspects of Electron Microscopy And Microbeam Analysis*, eds. B. M. Siegel and D. R. Beaman, Wiley, New York, 1975, pp. 205-239.
29. M. Sawamura, Y. Kuninobu, M. Toganoh, Y. Matsuo, M. Yamanaka and E. Nakamura, *J. Amer. Chem. Soc.*, 2002, 124, 9354-9355.
30. Y. Matsuo, Y. Kuninobu, S. Ito and E. Nakamura, *Chem. Lett.*, 2004, 33, 68-69.
31. T. W. Chamberlain, J. C. Meyer, J. Biskupek, J. Leschner, A. Santana, N. A. Besley, E. Bichoutskaia, U. Kaiser and A. N. Khlobystov, *Nat. Chem.*, 2011, 3, 732-737.
32. A. N. Khlobystov, *ACS Nano*, 2011, 5, 9306-9312.
33. F. Banhart, *Rep. Prog. Phys.*, 1999, 62, 1181-1221.
34. L. Guan, Z. Shi, M. Li and Z. Gu, *Carbon*, 2005, 43, 2780-2785.